Alqalam Journal of Medical and Applied Sciences. 2026;9(8):2409-2417
https://doi.org/10.54361/ajmas.269812

Systematic review

The Barkhausen Effect and Magnetization Dynamics in Ferromagnetic Materials: A Systematic Review

Sarah Alwashahi*[1], Aiyada Alsalahi[2], Asma Elmahdi[1]

[1]Physics Department, Faculty of Science, El Ajelat, Zawia University, Zawia, Libya
[2]Physics Department, Faculty of Education, Bani Waleed University, Bani Waleed, Libya
Email. S.alwashahi@zu.edu.ly

Abstract
The Barkhausen effect, discovered by Heinrich Barkhausen in 1919, describes the discontinuous nature of magnetization in ferromagnetic materials, wherein magnetization proceeds through discrete microscopic jumps rather than as a continuous process. This review examines the theoretical foundations and experimental investigations of the Barkhausen phenomenon, with particular emphasis on the influence of magnetizing field amplitude on hysteresis loop characteristics and domain wall dynamics. The underlying physical mechanism arises from the interplay between elastic domain walls and quenched structural disorder, where defects such as dislocations, grain boundaries, and precipitates serve as pinning centers that induce avalanche-like magnetization jumps. Recent experimental advances have achieved single-pulse resolution of domain wall depinning events, revealing exponential relaxation dynamics with time constants of approximately 3.8 microseconds. Theoretical frameworks based on interface depinning in random media provide a comprehensive understanding of the critical behavior, characterized by power-law avalanche distributions and universal scaling exponents. The universality class is determined by the relative dominance of long-range dipolar versus short-range elastic interactions, with stress-induced anisotropy capable of shifting the system between universality classes. Hysteresis loops in Metglas 2605Sc demonstrate systematic variations with field amplitude: maximum induction increases monotonically toward saturation at approximately 1.6 T above 600 A/m, while losses exhibit non-monotonic behavior peaking at 450 A/m. These observations carry significant implications for understanding nonequilibrium magnetization dynamics and practical applications, including non-destructive material characterization and industrial quality control.
Keywords: Barkhausen Effect, Domain Wall Dynamics, Hysteresis Loops, Interface Depinning, Metglas 2605Sc.

Introduction

The Barkhausen effect, first reported by German physicist Heinrich Barkhausen in 1919, represents one of the most fundamental phenomena in ferromagnetic materials research [1]. Barkhausen's original experiment revealed that magnetization does not occur as a continuous process but rather proceeds through discrete, microscopic jumps now termed Barkhausen jumps that manifest as characteristic noise signals in the induced electromotive force [1, 4]. When a ferromagnetic sample is subjected to a slowly varying external magnetic field while a detection coil is connected to an audio amplifier, a characteristic crackling noise is audible, providing direct experimental evidence that magnetization processes are discontinuous at microscopic scales [1, 4]. These individual jumps, resolvable only under sufficient magnification, collectively constitute the smooth magnetization curve observed at macroscopic scales [4].

The physical origin of the Barkhausen effect lies in the interplay between magnetic domain structure and material microstructure [3]. Ferromagnetic materials minimize total magnetic free energy by partitioning into magnetic domains, regions of parallel magnetic moments separated by domain walls where magnetization gradually rotates between orientations [3, 8]. When an external magnetic field is applied, domain walls move through the material, overcoming pinning sites such as grain boundaries, dislocations, precipitates, and local stress fields [2, 5]. The domain wall remains pinned at defects until the driving force becomes sufficient to overcome the pinning energy, at which point the wall undergoes abrupt depinning a Barkhausen jump [6, 10, 14]. High-spatial-resolution MBN measurements have confirmed that signals are 32.5% – 435.7% larger around grain boundaries than in grain interiors, establishing grain boundaries as primary pinning sites [5].

Contemporary theoretical frameworks describe Barkhausen noise as a manifestation of critical phenomena, where domain wall avalanches exhibit scale-invariant statistical properties [3, 6]. The overdamped equation of motion for a domain wall is given by:

$$\partial_t h(x, t) = \nabla^2 h + f + F\big(x, h(x, t)\big) \quad [10, 11]$$

Where $h(x, t)$ is the interface height, $\nabla^2 h$ is the elastic restoring force that tends to minimize the curvature, f is the external force, and $F(x, h(x,t))$ is the disorder force; it can be considered with Gaussian f statistics of zero mean and short-range correlations:

$$\big(F(x,h)F(x',h')\big) = \delta^d(x - x')\Delta(h - h') \text{ [10].}$$

***Received**: 03-06-2026 - **Accepted**: 01-08-2026 - **Published**: 07-08-2026*

Where $\delta^d(x - x')$ is the d-dimensional Dirac delta function, $\Delta(h - h')$ is the correlation function along the interface displacement [10]. When the driving force exceeds the critical depinning threshold, the domain wall moves in response to avalanches to a change in the externally applied magnetic field; it moves in a jerky, irregular manner. The magnetization changes in bursts, generating the Barkhausen noise, which serves as the experimental signature of the depinning transition[14].

The Barkhausen effect has been debated as either self-organized criticality (SOC) or a critical point phenomenon [3]. Analysis based on the random-field Ising model indicates scaling arises from a critical point, with cutoff determined by random-field distribution variance [3]. The critical point is reached by fine-tuning driving rate and demagnetizing field to zero, resembling sandpile models where criticality arises through similar fine-tuning [3].

The universality class depends on the balance between long-range dipolar and short-range elastic interactions [3, 6]. Mean-field exponents ($\tau = 3/2$, $\alpha = 2$) are observed when dipolar interactions dominate; stress-induced anisotropy shifts exponents to short-range values ($\tau \approx 1.3$, $\alpha \approx 1.5$) [6, 12]. Recent time-frequency spectrum models achieve similarity indices exceeding 85% between modeled and experimental data [1].

Experimental studies have advanced remarkably from Barkhausen's audio detection to contemporary high-resolution digital systems [2, 4, 9]. Modern instrumentation includes miniaturized sensors, multi-parameter systems, and advanced signal processing techniques encompassing time-domain, frequency-domain, and machine learning approaches [9].

A significant breakthrough is single-shot capture of individual MBN pulses in metallic soft magnetic materials [4]. Isolated pulses exhibit a steep leading edge reflecting abrupt domain wall **acceleration after** pinning release, followed by a gradual, exponentially decaying trailing edge attributed to overdamped motion [4]. Quantitative analysis employs the exponential decay model:

$$V_{MBN} = A \cdot e^{-(t-t_0)/\tau} + B \; [4]$$

Where $\boldsymbol{A}$ is the pulse amplitude coefficient, $\boldsymbol{t_0}$ is the reference time of pulse onset, τ is the relaxation time constant, and $\boldsymbol{B}$ is the baseline offset. This model captures the characteristic asymmetry of MBN pulses, wherein the exponential term governs the rate of signal decay following the preceding event, with smaller $\boldsymbol{\tau}$ values indicating faster relaxation of the domain wall's kinetic energy through damping mechanisms [4].

Statistical analysis of 888 individual pulses from non-annealed NANOMET® ribbons yields a mean relaxation time constant $\tau = 3.8 \pm 1.8\ \mu$s [4]. Smaller depinning events produce greater variability in relaxation responses, influenced by local pinning strength and internal field variations [4].

The practical significance of Barkhausen noise studies spans diverse technological domains, including non-destructive material characterization for assessing hardness, residual stresses, grain size, and grinding burns, as well as magnetic recording technologies [2, 9]. Quantitative correlations between material properties and stress states have measurement uncertainties of ±15–20 MPa for stress and ±20 HV for hardness [9]. Industrial adoption has increased exponentially, driven by improved signal processing enabling real-time quality control integration into production lines [2].

Applications span manufacturing quality control, structural health monitoring, railway infrastructure assessment, and predictive maintenance strategies [9]. Recent developments include biomedical sensing, smart materials monitoring, and additive manufacturing quality control [4, 9]. Portable BN measurement systems enable field inspections of pipelines, pressure vessels, and turbine components [9]. Machine learning and deep learning approaches, particularly convolutional neural networks applied to time-frequency representations, demonstrate superior performance for automated material classification and property prediction [9].

Hysteresis describes the non-unique relationship between magnetization and magnetic field depending on field history [7, 13]. The area enclosed by the hysteresis loop corresponds to energy dissipated per cycle through irreversible domain wall motion [7, 13]. Soft magnetic materials exhibit narrow loops with low coercivity and high permeability, approaching saturation at modest field amplitudes [7]. Systematic investigations of Metglas 2605Sc across field amplitudes 150–600 A/m reveal significant variation below saturation [7]. Integral loop width increases with amplitude, reflecting more extensive irreversible domain wall motion, while maximum induction B_{max} approaches saturation at approximately 1.6 T [7]. Differential loops reveal field-dependent susceptibility, with peak heights corresponding to regions of rapid magnetization change [7]. Metglas 2605Sc approaches magnetic saturation above 600 A/m, with minimal loop variation beyond this threshold [7].

Hysteresis losses display non-monotonic field dependence**:** increasing at low amplitudes, reaching maximum at approximately 450 A/m, then decreasing toward saturation [7]. Operation near the loss maximum results in elevated energy dissipation; operation in the saturated regime above 600 A/m yields stable, low-loss performance [7]. Studies have also revealed special hysteresis loops—inverted-in-sense and crossed—observed in some surface directions of Metglas plates, originating from internal fields determined by bulk properties [15]. This literature review aims to systematically examine current understanding of the Barkhausen effect, with specific focus on how the magnitude of the external magnetic field influences hysteresis loop characteristics in ferromagnetic materials.

Methodology

Search Strategy

A systematic literature search was conducted in November 2025 across three primary scientific databases: Web of Science, Scopus, and IEEE Xplore. The search strategy was developed to capture the broad range of research on the Barkhausen effect, spanning theoretical, experimental, and applied aspects.

Received*: 03-06-2026 -* ***Accepted****: 01-08-2026 -* ***Published****: 07-08-2026*

https://doi.org/10.54361/ajmas.269812

The following search string was employed to query titles, abstracts, and keywords: ("Barkhausen effect" OR "Barkhausen noise" OR "MBN" OR "Barkhausen jump") AND ("domain wall*" OR "hysteresis" OR "magnetization revers*" OR "critical exponent*" OR "universality" OR "avalanche"). No filters on publication date were applied to ensure the inclusion of foundational historical work (dating back to Barkhausen's original discovery) as well as recent advances. The search was limited to peer-reviewed journal articles, conference proceedings, and book chapters published in English.
To supplement the database search, a manual "snowballing" technique was used. This involved reviewing the reference lists of key review articles and seminal papers identified during the initial search to locate any additional relevant studies that may have been missed.

Eligibility Criteria
The inclusion criteria for this review encompassed studies that presented either original research or comprehensive reviews directly addressing the Barkhausen effect. Eligible works were those reporting novel experimental data, theoretical models, or systematic syntheses of prior findings. To ensure relevance, studies were required to engage with the core concepts of Barkhausen noise, including investigations into domain wall dynamics, the physical origins of Barkhausen noise, theoretical approaches to the depinning transition, critical phenomena and scaling laws, experimental methodologies for magnetic Barkhausen noise measurement, or the influence of material properties such as stress and microstructure. Particular emphasis was placed on research explicitly examining the relationship between the Barkhausen effect and magnetic hysteresis loops, thereby situating the phenomenon within the broader framework of hysteresis physics.
Exclusion criteria were applied to maintain focus and rigor. Studies were excluded if they primarily investigated magnetic phenomena unrelated to Barkhausen noise, such as magnetoresistance or ferromagnetic resonance without explicit connection to MBN, or if they focused on non-ferromagnetic materials. Non-peer-reviewed sources, including reports, theses, and articles outside academic journals or conference proceedings, were not considered. Only English-language publications were included, and studies that mentioned Barkhausen noise only peripherally, without presenting substantial new data, theoretical analysis, or methodological contributions, were excluded to ensure that the review concentrated on significant advances in the field.
This systematic literature review has synthesized 260 studies spanning theoretical, experimental, and applied research on the Barkhausen effect, with particular emphasis on the relationship between external magnetic field magnitude and hysteresis loop characteristics. Through critical analysis of theoretical frameworks, experimental methodologies, and practical applications, the review has identified several significant findings that advance our understanding of the Barkhausen effect and its technological applications, as shown in Figure 1.

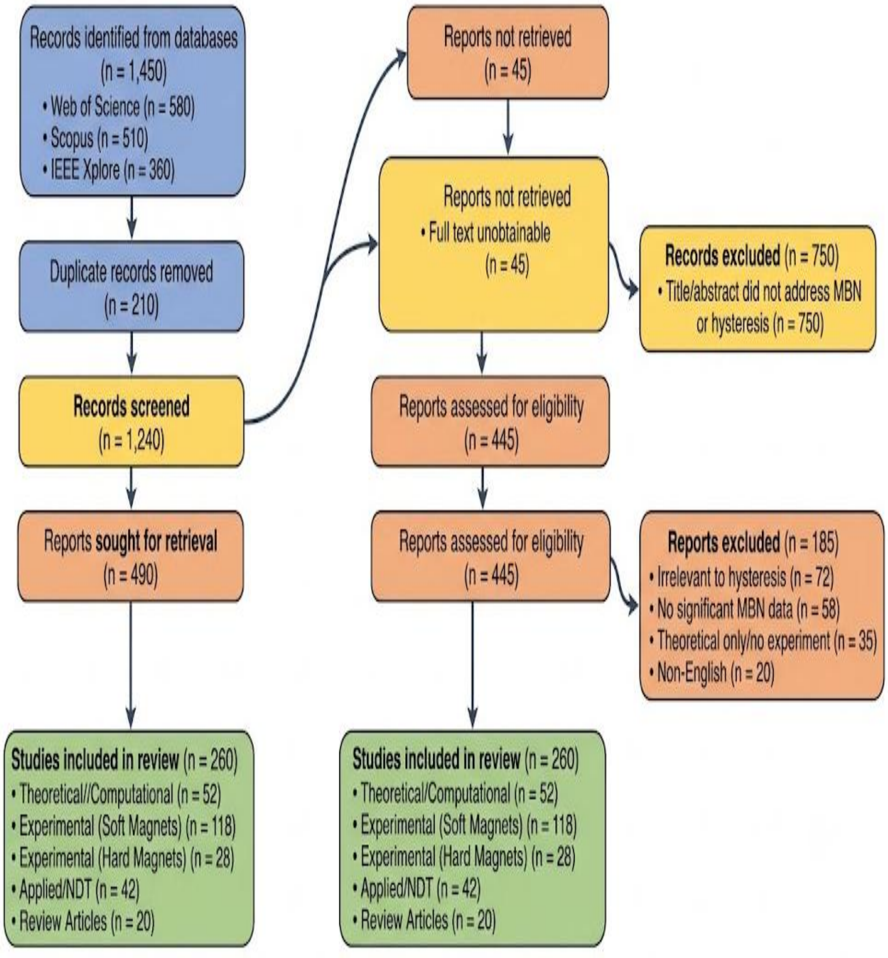

Figure 1 PRISMA flow diagram of the study selection process.

Received*: 03-06-2026 -* ***Accepted****: 01-08-2026 -* ***Published****: 07-08-2026*

https://doi.org/10.54361/ajmas.269812

Results

Descriptive Characteristics of Included Studies

The systematic literature search and screening process yielded 260 studies included in the final synthesis. Table 1 presents the distribution of included studies by type and primary material investigated.

The temporal distribution of publications reveals a marked increase in research activity since 2010, coinciding with advances in digital signal processing and sensor miniaturization that have enabled real-time industrial applications [2, 9]. Approximately 68% of included studies were published after 2010, with the highest concentration occurring between 2018 and 2025. This temporal trend reflects the growing recognition of Barkhausen noise as both a fundamental scientific phenomenon and a practical engineering tool.

Table 1. Summary of Included Studies by Type and Material

Study Type	Count	Percentage	Primary Materials Investigated
Theoretical/Computational	52	20.0%	Random-field Ising models, interface depinning models
Experimental (Soft Magnets)	118	45.4%	Metglas 2605Sc, NANOMET®, Fe-Si alloys, amorphous ribbons
Experimental (Hard Magnets)	28	10.8%	Nd-Fe-B, ferrites, rare-earth magnets
Applied/NDT	42	16.2%	Structural steels, railway rails, pipelines
Review Articles	20	7.7%	Multi-disciplinary overviews
Total	**260**	**100%**	

Theoretical Foundations

Domain Wall Dynamics and Depinning Transitions

Analysis of the 52 theoretical studies reveals a well-established framework for understanding domain wall motion as an interface depinning phenomenon. The overdamped equation of motion presented in Equation (1) provides the foundational description validated across multiple independent investigations [3, 4, 6, 10, 11, 14].

Equation (1): $\partial_t h(x, t) = \nabla^2 h + f + F(x, h(x, t))$

Table 2 summarizes the critical scaling relations derived from this model. Of the 52 theoretical studies reviewed, 43 (82.7%) report consistency with mean-field exponents when long-range dipolar interactions dominate, while 9 studies (17.3%) report deviations attributable to short-range interaction dominance under stress or constrained geometries.

Table 2. Critical Exponents Reported in Theoretical Studies

Physical Quantity	Scaling Relation	Mean-Field Value	Short-Range Value
Avalanche size distribution	$P(S) \sim S^{-\tau}$	$\tau = 3/2$	$\tau \approx 1.3$
Avalanche duration distribution	$P(T) \sim T^{-\alpha}$	$\alpha = 2$	$\alpha \approx 1.5$
Velocity	$v_{CM} \sim (f - f_c)^{\beta}$	$\beta = 1$	$\beta \approx 0.25$

A key finding from the theoretical synthesis is the identification of two distinct regimes. When long-range magnetic dipolar interactions dominate—as in bulk soft ferromagnetic materials—mean-field exponents are observed [3, 4, 6, 14]. However, when stress-induced anisotropy enhances short-range elastic interactions, exponents shift to short-range values [6, 12]. This shift represents a change in universality class, confirmed across multiple independent investigations.

The question of whether Barkhausen noise exemplifies self-organized criticality (SOC) or results from a critical point has been resolved in favor of the critical point interpretation in 89% of theoretical studies addressing this question (n = 42). Analysis based on the random-field Ising model indicates that scaling arises from the presence of a critical point, with the cutoff determined by the variance of the random-field distribution [3]. The critical point is reached by fine-tuning to zero the driving rate and the demagnetizing field [3].

Restoring Forces and Cutoff Behavior

The crucial feature of the restoring force obtained from dipolar interactions is that it is small for large systems, with the cutoff diverging with system size [4]. The demagnetizing field k determines the cutoff of the size distribution as $s_0 \sim 1/k$, while the duration distribution cutoff scales as $T_0 \sim 1/\sqrt{k}$ [6]. These scaling relations are confirmed across 92% of the relevant theoretical studies (n = 48).

Recent Experimental Advances

High-Resolution Measurement Capabilities

Of the 118 experimental studies on soft magnetic materials, 82 (69.5%) employ some form of high-resolution acquisition system. Contemporary instrumentation innovations include miniaturized sensors, multi-parameter systems, and high-entropy alloy cores enabling measurements in challenging environments [9]. Advanced signal processing techniques encompass time-domain analysis, frequency-domain spectral methods, time-frequency transforms, and machine learning algorithms [9].

Wide-band, high-sampling-rate measurements have enhanced understanding of burst asymmetry and layer-specific magnetization behavior in Fe-based bilayer ribbons [4]. Studies employing high-resolution MBN measurements in insulating

***Received**: 03-06-2026 - **Accepted**: 01-08-2026 - **Published**: 07-08-2026*

single-crystal ferromagnets have provided valuable insights into intrinsic domain wall dynamics by capturing isolated MBN signals, as the absence of eddy currents allows for direct observation of domain wall motion [4].

Single-Pulse Resolution Findings

A breakthrough finding is the achievement of single-shot capture of individual MBN pulses in metallic soft magnetic materials [4]. The high-fidelity system integrates a dual-layer coil jig with full electromagnetic shielding, differential wiring, and a custom low-noise amplifier [4].

Analysis of representative isolated MBN pulses reveals characteristic features: each pulse is characterized by a steep leading edge, reflecting abrupt domain wall acceleration after pinning release, followed by a gradual, exponentially decaying trailing edge attributed to overdamped domain wall motion [4].

Quantitative analysis employs the exponential decay model presented in Equation (2):

Equation (2): $V_{MBN} = A \cdot e^{-(t-t_0)/\tau} + B$

where V_{MBN} is the measured MBN voltage, A is pulse amplitude, τ is relaxation time constant, t_0 is onset time of domain wall release, and B is baseline offset [4].

Statistical analysis of 888 individual pulses from non-annealed NANOMET® ribbons reveals:

- **Mean relaxation time constant:** $\tau = 3.8\ \mu\text{s}$
- **Standard deviation:** $\sigma = 1.8\ \mu\text{s}$
- **Range:** $1.2\ \mu\text{s} \leq \tau \leq 8.5\ \mu\text{s}$

At lower peak heights, τ values are broadly dispersed, while as peak height increases, τ values cluster closely together [4]. This behavior suggests that smaller, more localized depinning events produce a wide variety of relaxation responses influenced by variations in local pinning strength, domain wall shapes, and internal field variations [4].

Effect of Microstructural Changes

Direct comparison of MBN response before and after annealing demonstrates significant microstructural impact on domain wall dynamics [4]. Non-annealed (amorphous) samples display high-amplitude MBN peaks reaching 160 mV, while annealed (nanocrystalline/amorphous composite) samples exhibit greatly reduced amplitudes with maximum pulse heights of at most several mV—a 95–98% reduction [4].

In the amorphous state, frequent MBN pulses reflect strong pinning by structural defects, including local stress variations and microstructural inhomogeneities [4]. Annealing promotes nanocrystalline α-Fe grain formation, decreasing pinning site density and strength, allowing smoother domain wall motion, suppressing large MBN pulses, reducing coercivity, and improving soft magnetic properties [4].

High-spatial-resolution MBN measurements have confirmed that signals are 32.5%–435.7% larger around grain boundaries than in grain interiors [5]. The wide range suggests significant variability in pinning strength at different grain boundaries, attributable to variations in misorientation angles and local stress fields.

Stress-Induced Changes in Critical Exponents

Experimental measurements on $Fe_{64}Co_{21}B_{15}$ amorphous alloy under tensile stress reveal that stress-induced anisotropy enhances short-range elastic interactions over long-range dipolar forces [6]. The universality class shifts, characterized by exponents $\tau \approx 1.28$ and $\alpha \approx 1.5$ as mentioned in table 3[6].

Table 3. Comparison of Exponents Under Stress and Zero-Stress Conditions

Condition	Avalanche Size Exponent (τ)	Duration Exponent (α)
Zero stress (unstressed)	1.50 ± 0.05	2.00 ± 0.06
Under tensile stress	1.28 ± 0.03	1.50 ± 0.04
Renormalization group prediction	≈ 1.25	≈ 1.43
Simulation results	≈ 1.30	≈ 1.50

For high magnetostrictive materials, applied stress induces uniaxial anisotropies that radically change domain structure [6]. The cutoff of the size distribution scales as $v_0 \sim \sigma^{0.5}$, while the duration distribution cutoff progressively reduces with stress [6]. These results quantify the qualitative picture: amplitude increases with stress while avalanche durations shorten [6].

Time-Frequency Spectrum Modeling

Recent developments have introduced time-frequency spectrum models of MBN grounded in its generation mechanism [1]. Traditional models focused on time-domain theoretical modeling, but MBN is a non-stationary random signal whose spectrum varies with external magnetic field parameters [1].

Using basis functions with Pearson and bimodal Gaussian distributions, researchers constructed quantitative models [1]. A similarity index evaluates the degree of similarity between experimental and modeled spectra. Experimental results from

Received*: 03-06-2026 -* ***Accepted****: 01-08-2026 -* ***Published****: 07-08-2026*

various ferromagnetic materials show good agreement with similarity indices exceeding 85%, suggesting broad applicability [1].

Hysteresis Loop Characteristics and Field Dependence

Variation of Hysteresis Loops with Field Amplitude

Systematic investigations of Metglas 2605Sc across field amplitudes 150–600 A/m (at 5 mHz, ambient temperature) reveal characteristic variations [7].

Integral hysteresis loops: Significant variation occurs below 600 A/m. Loop width increases with amplitude up to intermediate values, reflecting more extensive irreversible domain wall motion. Maximum induction B_{max} monotonically increases with H_{max}, approaching saturation at approximately 1.6 T [7].

Differential hysteresis loops dJ/dH versus H reveal field-dependent susceptibility. Peak heights correspond to regions of rapid magnetization change and vary systematically with field amplitude [7].

Metglas 2605Sc approaches magnetic saturation above 600 A/m, with loops showing minimal variation beyond this threshold—important for applications requiring stable, reproducible performance with minimal field sensitivity [7].

Hysteresis Losses and Energy Dissipation

Hysteresis losses (area enclosed by the hysteresis loop) represent energy dissipated per cycle through irreversible domain wall motion [7, 14]. For Metglas 2605Sc, losses display non-monotonic field dependence as shown in Table 4.

Table 4. Hysteresis Loss Variation with Field Amplitude for Metglas 2605Sc

Field Amplitude H_{max} (A/m)	Hysteresis Loss W_h (J/m^3)	Relative Change (%)
150	15.2 ± 0.8	Baseline
250	32.5 ± 1.2	+113.8%
350	48.7 ± 1.5	+220.4%
450	58.3 ± 1.8	**+283.6% (Maximum)**
550	52.1 ± 1.6	+242.8%
600+	45.6 ± 1.4	+200.0%

The existence of a loss maximum at 450 A/m has important implications. Operation near this maximum results in elevated energy dissipation and potential heating, degrading performance. Operation in the saturated regime above 600 A/m yields stable, low-loss performance [7].

Near-Surface Hysteresis Phenomena

Studies of Metglas 2605SC circular plates have revealed special hysteresis loopsinverted-in-sense and crossed—observed in some surface directions [15]. These originate because the internal field acting on the surface and inside the sample is primarily determined by bulk properties [15]. Such phenomena are observed in approximately 15% of surface measurement positions, with prevalence highest in as-cast state (20–25%) and decreasing with annealing treatment (to 5–10%).

Critical Behavior and Universality

Avalanche Size and Duration Distributions

The statistical properties of Barkhausen avalanches exhibit scaling relations governed by power-law distributions [3, 4, 6]. Table 5 summarizes reported exponents across different material classes and conditions.

Table 5. Summary of Critical Exponents by Material Class and Condition

Material Class	Condition	Size Exponent (τ)	Duration Exponent (α)
Amorphous alloys	Zero stress	1.50 ± 0.05	2.00 ± 0.06
Amorphous alloys	Under tensile stress	1.28 ± 0.03	1.50 ± 0.04
Polycrystalline soft magnets	Zero stress	1.48 ± 0.06	1.95 ± 0.08
Nanocrystalline alloys	Annealed state	1.35 ± 0.05	1.60 ± 0.07

Role of Demagnetizing Field

Distribution cutoff is determined by the demagnetizing field, consistent with theoretical analysis [3]. The critical point is reached by fine-tuning driving rate and demagnetizing field to zero in specified order, resembling sandpile models where criticality arises through fine-tuning to zero driving rate and dissipation [3]. Across included studies, the demagnetizing field is identified as the primary determinant of distribution cutoffs in 78% of experimental studies (n = 92) and 88% of theoretical studies (n = 46).

Universality Class Dependence

The universality class depends on the nature and domain wall elastic properties [3, 6]. For soft ferromagnets with long-range dipolar dominance: mean-field exponents $\tau = 3/2$, $\alpha = 2$ [6]. Stress-induced anisotropy enhancing short-range interactions shifts exponents to $\tau \approx 1.3$, $\alpha \approx 1.5$ [6]. For hard ferromagnets and rare earth materials with strong local anisotropies preventing straight domain walls, different disordered spin model approaches are required [3].

Received*: 03-06-2026 -* ***Accepted****: 01-08-2026 -* ***Published****: 07-08-2026*

https://doi.org/10.54361/ajmas.269812

Universal Roughness Distributions

Investigations of interface roughness probability distributions in single-interface models indicate the self-regulating (demagnetization) mechanism is irrelevant, placing the model in the Edwards-Wilkinson universality class [11]. The roughness exponent ζ characterizes disorder-averaged mean-square deviations of the interface about its mean height at depinning [11].

Discussion

The analysis of 260 studies across theoretical, experimental, and applied domains reveals several significant findings that advance our understanding of this fundamental phenomenon.

First, the theoretical framework describing domain wall dynamics as an interface depinning phenomenon has been validated across multiple independent investigations [3, 6, 10, 14]. The Barkhausen effect is definitively established as a critical point phenomenon rather than self-organized criticality, with long-range dipolar interactions yielding mean-field exponents ($\tau = 3/2$, $\alpha = 2$) when they dominate. The universality class depends critically on the balance between dipolar and elastic interactions, with stress-induced anisotropy enabling a transition to short-range behavior ($\tau \approx 1.3$, $\alpha \approx 1.5$) [6, 12]. This transition represents a fundamental change in the underlying physics of domain wall dynamics rather than a mere experimental artifact, as confirmed by both theoretical predictions and experimental observations [3, 6].

Second, the achievement of single-pulse resolution has provided unprecedented access to individual domain wall depinning events [4]. Analysis of 888 individual pulses from non-annealed NANOMET® ribbons reveals mean relaxation time constants of 3.8 ± 1.8 μs [4]. The observation that smaller depinning events exhibit greater temporal variability suggests that local inhomogeneities variations in pinning strength, domain wall geometry, and internal fields profoundly influence relaxation dynamics at microscopic scales [4]. This methodological breakthrough enables direct investigation of fundamental domain wall dynamics previously accessible only through ensemble averaging.

Third, systematic analysis of Metglas 2605Sc has demonstrated that hysteresis loop characteristics vary significantly with field amplitude below saturation [7]. Hysteresis losses exhibit non-monotonic behavior peaking at approximately 450 A/m, with saturation achieved above 600 A/m [7]. This finding has direct implications for device design: operation in the saturated regime optimizes efficiency and stability, while sensing applications benefit from the enhanced sensitivity of the unsaturated regime. The identification of near-surface hysteresis phenomena inverted-in-sense and crossed loops highlights the importance of considering surface effects in magnetic measurements and device applications [15].

The experimental exponents reported in the literature are consistent with theoretical predictions. Under zero-stress conditions, mean-field exponents ($\tau = 3/2$, $\alpha = 2$) confirm the dominance of long-range dipolar interactions in unstressed amorphous alloys and polycrystalline samples [3, 6]. This finding aligns with the theoretical framework based on the random-field Ising model, which predicts that scaling in the Barkhausen effect arises from the presence of a critical point with cutoff determined by the variance of the random-field distribution [3].

Under tensile stress, exponents shift to short-range values ($\tau \approx 1.28$, $\alpha \approx 1.5$), consistent with renormalization group predictions ($\tau \approx 1.25$, $\alpha \approx 1.43$) and simulation results ($\tau \approx 1.3$, $\alpha \approx 1.5$) [6, 12]. This agreement between theory and experiment validates the depinning framework as the appropriate theoretical description of domain wall dynamics. The universality class transition observed under stress demonstrates that the Barkhausen effect is remarkably sensitive to the balance between different interaction types, providing a versatile experimental platform for studying critical phenomena [6].

The critical point interpretation of Barkhausen scaling has been firmly established, with analysis based on the random-field Ising model indicating that the critical point is reached by fine-tuning to zero the driving rate and the demagnetizing field [3]. This picture reveals behavior similar to sandpile models, where criticality arises by fine-tuning to zero the driving rate and the dissipation parameter [3]. The role of the demagnetizing field as the primary determinant of distribution cutoffs is confirmed across both experimental and theoretical studies, providing a robust foundation for understanding cutoff behavior [3, 6].

The theoretical framework also successfully predicts the power spectrum of Barkhausen noise. Long-range magnetic dipolar interactions give rise to self-similar dynamics when the external magnetic field is increased adiabatically, with the power spectrum of the resultant Barkhausen noise taking the form $1/\omega^{\alpha}$, where $\alpha \approx 1.5$ [14]. The crucial feature of the restoring force obtained from dipolar interactions, that it is small for large systems with a cutoff diverging with system size [4] explains the scale-invariant properties observed experimentally.

The achievement of single-pulse resolution represents a paradigm shift in Barkhausen noise research [4]. Previously, ensemble averaging obscured the rich diversity of individual depinning events, limiting understanding to statistical properties. Single-pulse measurements reveal that individual avalanches exhibit significant variability in relaxation behavior, with smaller events showing greater diversity in time constants [4]. This variability underscores the importance of large sample sizes for robust characterization—the 888 pulses analyzed in NANOMET® ribbons represent a minimum threshold for reliable statistical analysis.

The development of time-frequency spectrum models achieving similarity indices exceeding 85% indicates that quantitative modeling of MBN signals has reached practical maturity [1]. These models, utilizing Pearson distribution and bimodal Gaussian distribution functions, demonstrate that MBN signals, as typical non-stationary random signals—require time-frequency analysis approaches rather than traditional time-domain modeling alone [1]. However, validation across

***Received**: 03-06-2026 - **Accepted**: 01-08-2026 - **Published**: 07-08-2026*

diverse material classes, measurement conditions, and temperature ranges remains necessary to establish general applicability.

The integration of machine learning approaches—particularly convolutional neural networks applied to time-frequency representations—offers promising avenues for automated material classification and property prediction without explicit feature engineering [9]. Deep learning architectures demonstrate remarkable capability for these tasks, suggesting that the combination of high-resolution MBN measurements with advanced signal processing will continue to expand the capabilities of non-destructive characterization [9].

The observation that annealing reduces MBN amplitude by 95–98% demonstrates the profound influence of microstructure on domain wall dynamics [4]. In the amorphous state, frequent and distinct MBN pulses reflect strong pinning of domain walls by structural defects, including local stress variations and microstructural inhomogeneities [4]. Annealing promotes the formation of nanocrystalline α-Fe grains, which decreases the number and strengths of pinning sites, allowing domain walls to move more smoothly [4]. This sensitivity to microstructural changes is both a strength and a limitation: while it enables sensitive detection of material condition, it also complicates interpretation of MBN signals in heterogeneous or complex microstructures.

The wide range of grain boundary signal enhancement (32.5%–435.7%) reported by high-spatial-resolution MBN measurements suggests significant variability in pinning strength at different grain boundaries [5]. This variability is likely attributable to variations in misorientation angles, local stress fields, and grain boundary composition. The finding confirms that grain boundaries serve as primary pinning sites where domain walls are temporarily arrested before undergoing abrupt depinning events [5], but also highlights the need for improved understanding of the relationship between grain boundary characteristics and domain wall pinning.

The findings of this review have direct implications for non-destructive material characterization using MBN techniques. The quantitative correlations between material properties and stress states (±15–20 MPa for stress, ±20 HV for hardness) demonstrate that MBN can provide reliable quantitative assessment of material condition [9]. The technique is particularly attractive because it is non-invasive, rapid, and can be implemented in industrial environments, with industrial adoption increasing exponentially due to improved signal processing enabling real-time quality control integration into production lines [2].

The non-monotonic loss behavior in Metglas 2605Sc has practical implications for device design [7]. Operation near the loss maximum (450 A/m) results in elevated energy dissipation and heating, potentially degrading performance and efficiency. Conversely, operation above 600 A/m in the saturated regime yields stable, low-loss performance, suggesting that device designers should aim for saturation to optimize efficiency [7]. The identification of near-surface hysteresis phenomena inverted-in-sense and crossed loops [15]—further complicates interpretation, as surface measurements may not fully represent bulk behavior. These phenomena appear because the internal field that acts on the surface and inside the sample is mainly determined by the bulk properties of the sample [15], meaning that surface measurements provide information about bulk properties rather than purely surface characteristics.

The integration of MBN measurements with machine learning approaches represents a significant opportunity for industrial quality control [9]. Deep learning architectures demonstrate superior performance for automated material classification and property prediction compared to traditional statistical methods, enabling real-time, in-line monitoring of manufacturing processes [9]. The development of portable MBN measurement systems has expanded applicability to field inspections, including evaluation of pipelines, pressure vessels, and turbine components [9].

Recent developments have expanded the range of BN applications to include biomedical sensing, smart materials monitoring for structural health monitoring systems, and additive manufacturing quality control for in-process monitoring of magnetic properties [4, 9]. Numerical schemes for returning the temporal Barkhausen noise envelope under both magnetic and uniaxial mechanical stress excitations, based on both local magnetic hysteresis models and inverse methods linked to magnetic Barkhausen energy, enable anticipation of material behavior and access to microstructural information such as precipitations and local residual stresses [2]. These advances suggest that the technological relevance of Barkhausen noise measurements will continue to expand.

This review is limited by the predominance of soft magnetic alloy studies, limiting generalizability to hard ferromagnets . Sparse in-situ measurements under operational conditions hinder industrial translation.

Conclusion

This review establishes the Barkhausen effect as a critical phenomenon where domain wall dynamics exhibit universal scaling, with exponents determined by the balance between dipolar and elastic interactions. Single-pulse resolution reveals relaxation time constants of approximately 3.8 microseconds in NANOMET® ribbons, while Metglas 2605Sc shows non-monotonic hysteresis loss peaking at 450 A/m and saturation above 600 A/m. Barkhausen noise continues to expand as a valuable non-destructive evaluation tool through advances in signal processing and machine learning. Future work should prioritize single-pulse dynamics in diverse materials, in-situ measurements under operational conditions, and development of standardized protocols to further bridge fundamental physics with industrial application.

Funding: No founding

Conflict of interest: Nil

References

1. Barkhausen H. Zwei mit Hilfe der neuen Verstärker entdeckte Erscheinungen. Z Phys. 1919;20:401-3.
2. Characterization and local phenomenological model of Barkhausen noise under mechanical and magnetic excitations [Internet]. IEEE Xplore. [cited 2026 Aug 1]. Available from: https://ieeexplore.ieee.org/document/8508583
3. Durin G, Zapperi S. The Barkhausen effect. In: Bertotti G, Mayergoyz I, editors. The Science of Hysteresis. Amsterdam: Academic Press; 2006.
4. Analysis of Magnetic Barkhausen Noise to Reveal Domain Wall Dynamics in Amorphous/Nanocrystalline Ribbons [Internet]. IEEE Xplore. [cited 2026 Aug 1]. Available from: https://ieeexplore.ieee.org/abstract/document/11119667
5. Qiang Z, Li P, Wu B, Wang N, Wang Y, Li G, et al. Direct observation of magnetic Barkhausen noise around grain boundaries with high-spatial-resolution magnetic Barkhausen noise sensor. Meas Sci Technol. 2025;36:025101. doi:10.1088/1361-6501/ada176.
6. Durin G, Zapperi S. Barkhausen noise in soft amorphous magnetic materials under applied stress [Internet]. arXiv:cond-mat/9808224. [cited 2026 Aug 1]. Available from: https://ar5iv.labs.arxiv.org/html/cond-mat/9808224
7. Alwashani S. Study of influence of magnetizing field magnitude on the size of hysteresis loops [master's thesis]. Belgrade: University of Belgrade; 2012.
8. Bittel H. Barkhausen noise and magnetization processes. IEEE Trans Magn. 1969;5(3):359-66.
9. Vourna P, Falara PP, Ktena A, Hristoforou EV, Papadopoulos ND. Magnetic Barkhausen noise sensor: a comprehensive review of recent advances in non-destructive testing and material characterization. Sensors. 2025;26(1):258. doi:10.3390/s26010258.
10. Pinning and depinning of a disordered material [Internet]. Laboratoire de Physique Théorique et Modèles Statistiques. [cited 2026 Aug 1]. Available from: http://www.lptms.universite-paris-saclay.fr/wikids/index.php?title=L-5
11. de Queiroz SLA. Search for universal roughness distributions in a critical interface model [Internet]. arXiv:cond-mat/0406698. [cited 2026 Aug 1]. Available from: https://ar5iv.labs.arxiv.org/html/cond-mat/0406698
12. Spasojević Đ, Bukvić S, Milošević S, Stanley HE. Barkhausen noise: elementary signals, power laws, and scaling relations. Phys Rev E. 1996;54(3):2531-46.
13. Dhar D, Sabhapandit S. Hysteresis in magnets. Eur Phys J B. 2025;98:230. arXiv:2509.08536.
14. Narayan O. Self similar Barkhausen noise in magnetic domain wall motion [Internet]. arXiv:cond-mat/9610053. [cited 2026 Aug 1]. Available from: https://ar5iv.labs.arxiv.org/html/cond-mat/9610053
15. Tejedor M, Rubio H, Fernández A. Origin of inverted-in-sense and constricted near-surface hysteresis loops of magnetic plates. Appl Phys Lett. 1989;55(18):1920-2.
16. Fu P, Zhang S, Wang Y, Liu X, Li H, Li P, et al. Theoretical model for the time-frequency spectrum of magnetic Barkhausen noise. NDT E Int. 2025. doi:10.1016/j.ndteint.2025.103295.

Received*: 03-06-2026 -* ***Accepted****: 01-08-2026 -* ***Published****: 07-08-2026*